International Journal of Heat and Mass Transfer 131 (2019) 487–494

Contents lists available at ScienceDirect

International Journal of Heat and Mass Transfer

journal homepage: www.elsevier.com/locate/ijhmt

A strategy of hierarchical particle sizes in nanoparticle composite for enhancing solar reflection

Joseph Peoples [a], Xiangyu Li [a], Yaobing Lv [b], Jun Qiu [a,b,c], Zhifeng Huang [d], Xiulin Ruan [a,*]

[a] School of Mechanical Engineering and the Birck Nanotechnology Center, Purdue University, West Lafayette, IN 47907, USA
[b] School of Energy Science and Engineering, Harbin Institute of Technology, Harbin 150001, China
[c] State Key Laboratory for Digital Manufacturing Equipment and Technology, Huazhong University of Science and Technology, Wuhan, Hubei 430074, China
[d] School of Power and Mechanical Engineering, Wuhan University, Wuhan, Hubei 430072, China

ARTICLE INFO

Article history:
Received 17 July 2018
Received in revised form 11 October 2018
Accepted 12 November 2018

ABSTRACT

A key requirement for achieving passive radiative cooling for an ideal emitter, in the sky window (8–13 μm), during daytime is a total solar reflection >85%, and every 1% above this threshold results in ~10 W/m^2 gain in cooling power. One promising, inexpensive, and scalable solution for achieving high total solar reflectance is a dielectric nanoparticle-polymer composite coating. Past works have widely used a single particle size. However, it is challenging to achieve solar reflectance significantly above 85%. Here, recognizing the broadband nature of the solar irradiation, we propose and test a new concept of enhancing solar reflection at a given particle volume concentration by using hierarchical particle sizes, which we hypothesize to scatter each band of the solar spectrum i.e. VIS, NIR, and UV effectively. The hypothesis is tested using a TiO_2 nanoparticle-acrylic system. Using the Mie Theory, the scattering and absorption efficiencies and asymmetric parameter of nanoparticles with different sizes and combinations are calculated, then the Monte Carlo Method is used to solve the Radiative Transfer Equation. When validating our computational model to in-house experimental results it is found that a nanoparticle size distribution of d = 104 ± 37 nm creates an overall better fit to the experimental data and increases the total solar reflection when compared to the single size model of d = 104 nm. We then purposely design hierarchical combinations of particle sizes in the broader range of 50 nm to 800 nm, and we have achieved an overall total solar reflection of ≈91%, which is higher than the ≈78% and ≈88% for 100 nm and 400 nm single particle sizes, respectively. The results confirm our hypothesis that hierarchical particle sizes can scatter over a broad spectrum more effectively rather than any single particle size. Moreover, our findings could also cut the manufacturing cost since no precise control of particle size is necessary.

1. Introduction

Active cooling accounted for 15% of the total residential energy consumption in the U.S. in 2017, and 9% of the total commercial energy consumption in the U.S. in 2012 [1]. There is a great need for more efficient methods of cooling, not only in North America but across Central America, Africa, and parts of Asia. Passive radiative cooling can help to address the need for efficient cooling technologies, in both the residential and commercial sectors. Radiative cooling is the process of creating an energy exchange between the system of interest and deep space, which is approximately 3 K, resulting in an infinite and extremely cold heat sink. This can be done by engineering spectrally selective surfaces with two primary functions. First, the surface must emit in the region where the atmosphere is transparent (8–13 μm), also known as the "sky window", leading to an efficient rejection of thermal energy to deep space. Second, the surface must be able to reflect incoming solar irradiation. When assuming an ideal emitter, with an emissivity of one in the sky window, the surface must reflect more than 85% of the incoming solar irradiance in order to achieve a net cooling effect and ever 1% above this threshold converts to a gain of ~10 W/m^2 of cooling power. Understanding that no surface will have an ideal emissivity and the cooling performance is attenuated by many factors (e.g. humidity, visibility, and advection), the threshold solar reflectance for achieving net cooling could be higher than 85%. Many materials seen in everyday life such as water, carbon, and many polymers have good emission properties in the sky window but are limited due to their insufficient capability of reflecting the sunlight [2]. Although investigations have been done on this topic for decades, recent advances in nanomaterials

* Corresponding author.
E-mail address: ruan@purdue.edu (X. Ruan).

https://doi.org/10.1016/j.ijheatmasstransfer.2018.11.059
0017-9310/

processing and a deeper understanding of electromagnetic interactions at the nanoscale have triggered renewed interest at a rapid pace.

Nanofabrication techniques have been employed for radiative cooling showing full daytime cooling below ambient temperatures. Raman *et al.* shows a 5 °C below ambient temperature during peak solar irradiation using a multi-layer thin film structure [3]. Gentle et al. created a stacked-polymer mirror with a silver backing achieving a more manufacturable radiative cooling coating for roofing applications that demonstrated below ambient temperatures for a 24-h period [4]. A scalable solution using nanoparticles as the emitters involved silica-TPX nanocomposite films with silver backing, providing 93 W/m^2 cooling power continuously through 24 h [5]. Kou et al. achieved full daytime cooling using a simple quartz layer-silver thin film structure [6]. However, these techniques are either expensive and not scalable solutions, or use metallic films to reflect solar irradiation where the metal can be expensive and hinder most communication EM frequencies, limiting their application space in the telecommunication field. Paints designed for radiative cooling purpose provide another nice option for scalability and ease of use. Nanocomposites involving TiO_2 are studied in the literature due to its high refractive index and low cost of fabrication [7-10]. Huang *et al.* proposed a dual-layer coating for daytime passive radiative cooling, using a TiO_2 acrylic nanocomposite on top for solar reflection and carbon black paint at the base for emission [11]. Atiganyanun *et. al.* optimizes the solar reflectance of randomly packed SiO_2 microspheres while maintaining high emissivity in the sky window achieving partial daytime cooling without a metallic bilayer [12]. These studies have widely used a single particle size; however, it is a very challenging task to achieve solar reflectance significantly above 85% which hinders full daytime cooling under direct sun. Strategies for achieving ultra-high solar reflectance are needed [13].

Here, recognizing the broadband nature of the solar irradiation, we hypothesize and test a new concept of enhancing solar reflection by using hierarchical particle sizes, which can scatter each band of the solar spectrum i.e. VIS, NIR, and UV effectively. Using the Mie Theory and a photon Monte Carlo method, we predict the reflectance of solar irradiation, on a TiO_2 nanoparticle-acrylic composite thin film as our model system [11]. When trying to match the computational results with experimental data on single-sized nanoparticles (as the vendor claims), the models underestimated solar reflection. However, when a narrow size distribution is considered, our model can fit the experimental data more accurately. Inspired by this and recognizing that the solar spectrum is broad, we hypothesize that intentionally using multiple particle sizes can scatter different parts of the solar wavelength effectively and increase the total solar reflectance than any single size. We then investigated a variety of size combinations, and the results confirmed our hypothesis. Although our results only considered the solar wavelength region, the principle of using multiple particle sizes to maximize the scattering and reflection of a broadband radiation will hold for any spectral region and impact many other fields.

2. Methodology

Investigating spectral reflectance of nanoparticle composites can prove to be a complex task, from both mathematical and computational cost perspective. There are many methods to achieve spectrally resolved reflectance of nanoparticle composites; each of them with their respective advantages and limitations. Solving Maxwell's equations directly would be mathematically cumbersome and computationally expensive [14]. A direct Monte Carlo method, where each particle location was recorded, and the light path was tracked, could be employed, but with the size of the domain and number of particles, the computational expense would be unfeasible. Therefore, this work combines the Mie theory, effective medium theory, and Monte Carlo method [11]. The particles are assumed to scatter independently of one another at low volume concentrations [15–18]. The scattering coefficient, absorption coefficient, and phase function of each individual particle are first calculated from the Mie Theory. The nanocomposite is then approximated as an effective medium with volume-averaged coefficients without tracking the positions of individual particles. The Radiative Transfer Equation is finally solved via the Monte Carlo method; reducing the computational expense.

2.1. Mie theory

The Mie Theory, also known as the Lorenz-Mie Theory, gives a set of governing equations to examine the interaction between an electromagnetic wave of wavelength, λ, and a spherical particle of diameter, d, with a complex index of refraction, $m = n + i\kappa$, when d is comparable to λ [15,16,19,20]. The complex index of refraction of the spherical particle needs to be corrected if the particles are suspended in a participating media, as the Mie Theory cannot directly handle participating media. This work will adopt the simple approach, following the notation in Bohren [15], where the complex index of refraction of the particle is divided by the index of the medium, n_0 [15,21,22], neglecting any matrix absorption. There are more accurate approaches for participating media that include the matrix absorption [17,23–27]. However, due to a lack of the dielectric function of acrylic in the literature and such information not provided by our vendor, this work does not implement these more accurate methods. This simplification could lead to up to 3% overestimation in the total solar reflectance [28], however, will not affect our main hypothesis or conclusion. There are two nondimensional parameters needed for the Mie Theory: the normalized complex index of refraction, $m = \frac{n+i\kappa}{n_0}$, and the size parameter, $x = \frac{\pi d}{\lambda}$. Our computational model is based on an open source code developed by Matzler [29], which is modified in the current work to accept multiple particle sizes.

The overall calculation procedure is similar to that presented by Zhifeng et al. [11] with modifications to include multiple particle sizes and is briefly summarized here. The scattering efficiency (Q_{sca}) and extinction efficiency (Q_{ext}) can be calculated using the Mie coefficients, and the absorption efficiency (Q_{abs}) is obtained by taking their difference. The asymmetric parameter for a single particle, which is needed for the Monte Carlo simulation, is obtained by [16]

$$g_s = Q_{sca}\langle cos\theta\rangle = \frac{4}{x^2}\left[\sum_{n=1}^{\infty}\frac{n(n+2)}{n+1}Re(a_n a_{n+1}^* + b_n b_{n+1}^*) + \sum_{n=1}^{\infty}\frac{(2n+1)}{n(n+1)}Re(a_n b_n^*)\right] \quad (1)$$

where x is the size parameter, a_n and b_n are the Mie coefficients [11,15,16], and the notation b_n^* represents the conjugate transpose of the b_n.

Next, we approximate the nanoparticle-polymer composite as an effective medium. The effective scattering and absorption coefficients, as well as the asymmetric parameter, can be found by

$$\sigma_T = \sum_{i=1}^{c}\frac{3f_i Q_{sca,i}}{2d_i} \quad (2)$$

$$\kappa_T = \sum_{i=1}^{c}\frac{3f_i Q_{abs,i}}{2d_i} \quad (3)$$

$$g_T = \frac{1}{\sigma_T}\sum_{i=1}^{c}\frac{3f_i g_{s,i} Q_{sca,i}}{2d_i} \tag{4}$$

where c is the number of different particle sizes used, while d_i and f_i are the diameter and volume concentration of each particle, respectively [16].

The scattering phase function provides the directional dependence of the scattering of the photon. After the scattering phase function for a single particle size $\Phi_s(\theta)$ is calculated [11,16], the scattering phase function of a nanocomposite containing multiple particle sizes can be calculated using [11,16]

$$\Phi_T(\theta) = \frac{1}{\sigma_T}\sum_{i=1}^{c}\frac{3f_i \Phi_{s,i}(r_i,\theta) Q_{sca,i}}{2d_i} \tag{5}$$

2.2. Monte Carlo for photon transport

Monte Carlo (MC) is a stochastic modeling method, using large quantities of random events to predict physical events rather than relying on analytical solutions. Many works implemented MC to solve the Radiative Transfer Equation [11,16,19,30]. Achieving accurate solutions for photon transport in an effective scattering medium using MC can still be quite computationally expensive; the model in this work release 1,000,000 photon packets into the medium per wavelength for 130 discrete wavelengths. The trajectory and energy of each photon packet is tracked to determine reflectance, transmittance, and reflectance. The computational code used for this work is an open source code developed by Wang et al. for modeling photon transport in multi-layer turbid tissue for cancer research [31]. The computational code is well documented and available online; therefore, the details will not be explained in this work.

3. Results and discussion

Understanding the source of the incident irradiance is the first step when trying to enhance the reflectance. For our applications, the source of irradiance is the attenuated solar irradiation, more specifically known as the standard terrestrial solar spectral irradiance at normal incidence air mass 1.5 (AM1.5) [32]. Fig. 1 shows the AM1.5 spectra up to $\lambda = 2.5\mu m$, as the irradiance at longer wavelengths contributes very little.

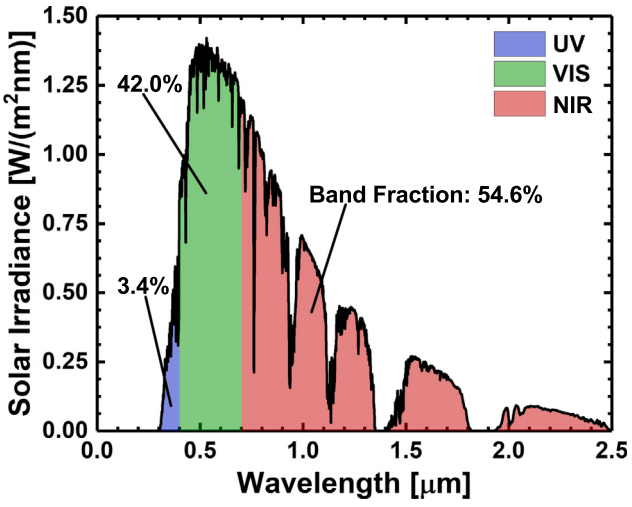

Fig. 1. Spectral solar irradiance based on AM1.5 [29], the UV, VIS, and NIR bands are highlighted and their respective contribution to the total solar irradiation given by the band fraction.

Fig. 1 gives a breakdown of the ultraviolet (UV), visible (VIS) and near-infrared (NIR) band contribution to the total solar irradiation, labeled as band fraction in the figure. Since the largest portion of total solar irradiance occurs in the NIR band, at 54.6%, it should be the first priority to be considered when optimizing the reflection of these coatings, but the 3.4% of the ultraviolet should not be neglected as 3.4% of an $\approx$1000 W/m^2 intensity is still a large amount of energy that needs to be reflected.

3.1. Single particle size

We have performed experiments on TiO_2 nanoparticle-acrylic composite films where the nanoparticle size is 100 nm as specified by the vendor US Research Nanomaterials, Inc. Therefore, we will model this system to compare with experiments. In addition, we have included a few other single sizes (25, 50, 200, 400, and 800 nm) to gain more insights. Fig. 2 shows the scattering and absorption coefficients for these single sized particles.

As we can see, the 100 nm and 200 nm nanoparticles have strong scattering peaks and low absorption coefficients in the VIS band, which are good indicators for strong reflection in the VIS band. The 400 nm particle size has a small yet broad scattering peak which is greater than all the particles sizes in the NIR band leading to high reflectance of solar irradiation in this region. As the particle size decreases, the scattering peak shifts to shorter wavelength (deep UV), but the absorption becomes stronger as well. The 25 nm size shows poor scattering over the entire solar region and very strong absorption, which is not ideal for our applications.

The likelihood of a particle reflecting a photon can be interpreted by its ability to backscatter the photon, and the scattering phase function helps to visualize the particle's capability to backscatter. There are three predominantly defined scattering regions, when referring to spheres interacting with photons: Rayleigh scattering, Mie scattering, and geometric scattering. If the particle is comparable to the wavelength of light it is in the Mie scattering region, then it predominately has a forward weighted scattering phase function. The Rayleigh scattering region is observed when the particle is much smaller than the wavelength of light, leading to a more equivalent forward versus backward scattering phase function. Geometric scattering is the region where the particle is much larger than the wavelength of light, creating a very dominant forward scattering phase function with well defined narrow regions of backscattering [16]. In Fig. 3A and B, the scattering phase functions for five particle sizes are shown at $\lambda = 480$ nm, excluding the 800 nm particle size as it is mostly geometric scattering, therefore, the large forward scattering it dominates making the other curves hard to distinguish. We can clearly see the differences between Rayleigh (at the smaller diameters) and Mie scattering (at the larger diameters). In Fig. 3B, we observe that the 400 nm particle size will create the greatest backscattering. The smaller diameter particles, 25 nm and 50 nm show decent backscattering; however, the results from above show that they have weaker scattering coefficients and higher absorption coefficients which are undesired for solar reflectance. The overall performance will depend on how these factors interplay, as will be discussed next.

Fig. 4A shows the spectral reflectance of six single size particles, with a 5% volume concentration embedded in acrylic with a film thickness of 1 mm, across the entire solar spectrum, and Fig. 4B shows the same data zoomed in to highlight the UV region. The 400 nm and 800 nm particle sizes have the best performance in the NIR band which should be the first priority when optimizing for total solar reflection. The 100 nm and 200 nm particle sizes have the largest peaks in the VIS band and the 100 nm and the 50 nm particle sizes perform the best in the UV band. Table 1 shows the total solar reflectance, calculated using the AM1.5

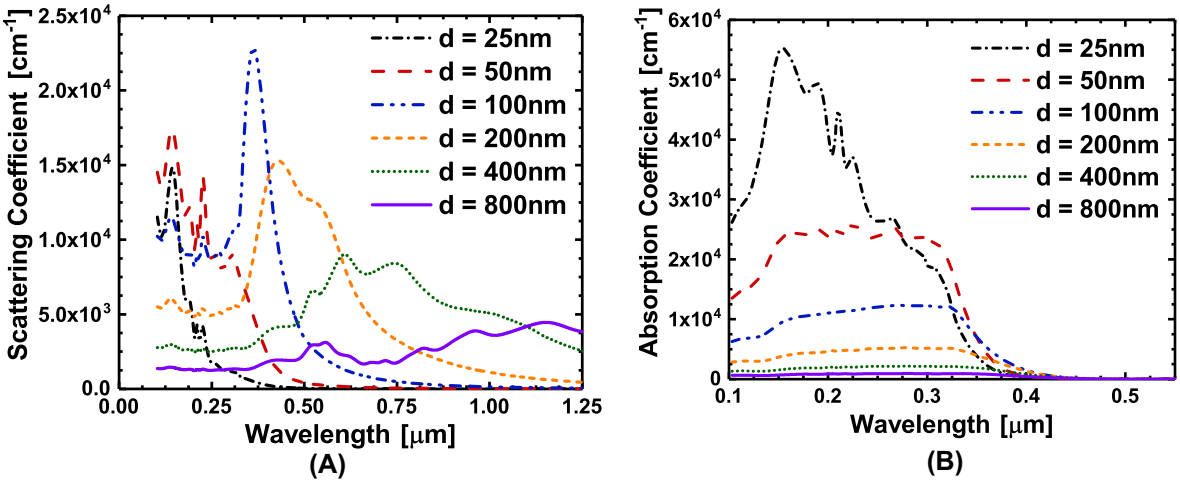

Fig. 2. (A) Scattering coefficient and (B) absorption coefficient for single size TiO_2 particles in at a volume fraction, $f = 5\%$ embedded in acrylic matrix.

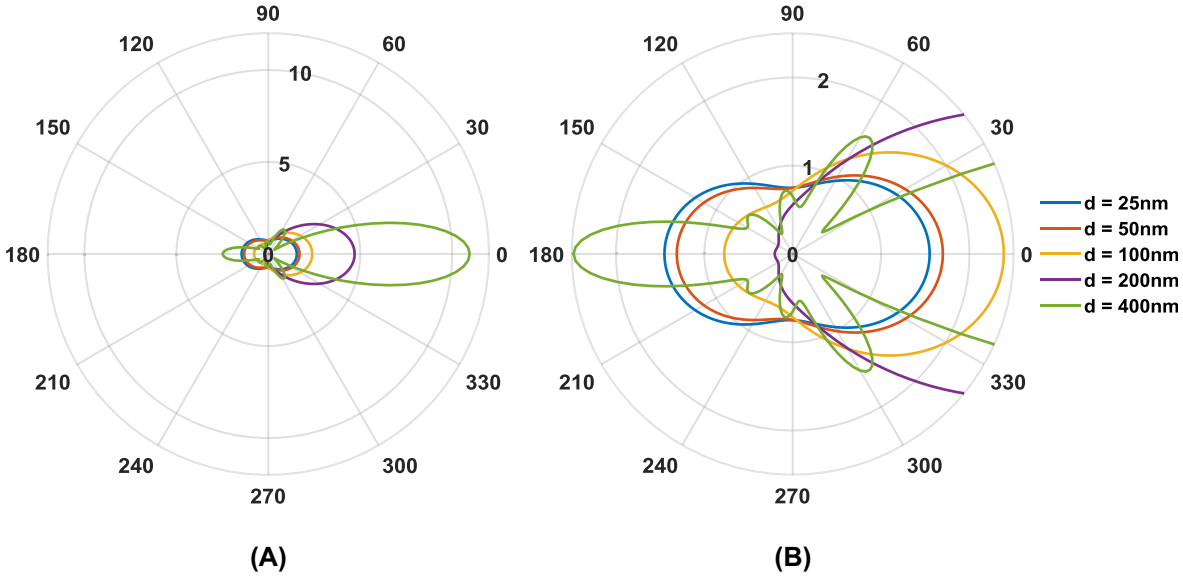

Fig. 3. (A) Scattering phase function at $\lambda = 480$ nm for single size TiO_2 particles and (B) a zoom in on the same scattering phase functions; all at a volume fraction, $f = 5\%$ embedded in acrylic matrix.

spectra mentioned earlier [32]. From Fig. 4B, it would look as if the 50 nm particle would have the greatest UV band reflection, however, this is not the case; it is actually the 100 nm particle that has the greatest UV band reflectance because the terrestrial solar irradiance begins at $\lambda = 280$ nm. The 50 nm does still have high UV band reflectance, when compared to the other particle sizes, and outperforms the others in the deep UV, but that is not of interest for our applications. The 200 nm size particle has the greatest VIS band reflectance, and the 400 nm size particle has the greatest NIR band reflectance which is why it has the greatest total solar reflectance. Of the six single size particles; the total solar reflectance values for the 200 nm and 400 nm particle sizes are within 0.3%, therefore it can be concluded that even if an optimal single size was found within this design space the improvement would be minimal. When trying to predict the particles spectral reflectance capabilities from the scattering and absorption coefficient, seen in Fig. 2A and B, the main takeaway is that the spectral location of the scattering coefficient peak, not necessarily its magnitude, coupled with a low absorption coefficient will have a high impact on overall performance.

3.2. Comparison with experimental results

TiO_2 acrylic nanocomposites were fabricated and tested for proof-of-concept radiative cooling experiments using $d \approx 100$ nm (specified by the vendor, US Research Nanomaterials, Inc.) TiO_2 nanoparticles at an $f_i = 8\%$, a 2 mm thick acrylic composite was fabricated. An SEM image of the TiO_2 nanoparticles used in these experiments can be seen in Fig. 5A, note that the nanoparticles have a thin (~2nm) coating on them to reduce charging effects. The actual size distribution was found to be $d = 104 \pm 37$ nm. The reflectance was then measured using a UV–VIS-NIR spectrometer with an integrating sphere, and the results can be seen in Fig. 5B. The total solar reflectance from the experimental data was calculated to be 90.1%. When comparing the experimental results with the modeling data, the predicted reflectance for a single particle size, $d = 104$ nm, is 84.2%, which is a significant underestimation. This indicates that using an average size fails to capture the correct radiation characteristics. To account for this size distribution, a random number generator was used to generate a set of sizes of particles that follow $d = 104 \pm 37$ nm while conserving the total

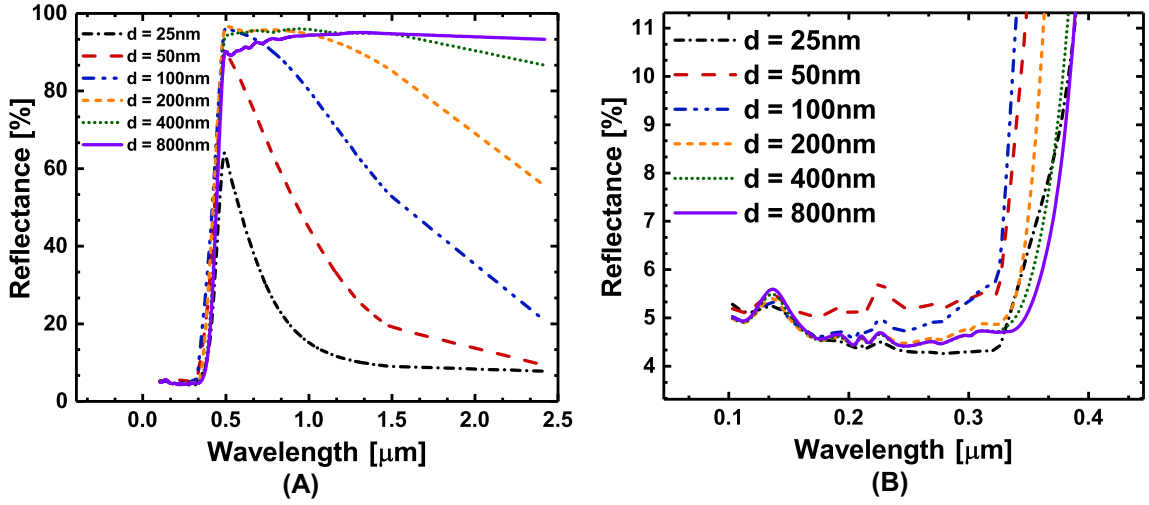

Fig. 4. (A) Spectral reflection over the entire solar region and (B) spectral reflection in the UV region for single size TiO_2 particles in at a volume fraction, $f = 5\%$ and 1 mm thickness embedded in acrylic matrix.

Table 1
Total solar reflectance values for single size particles; the total volume fraction is conserved at 5% and the thickness of each model is 1 mm.

Model (Single Size)	UV Band Reflectance: R_{UV} [%]	VIS Band Reflectance: R_{VIS} [%]	NIR Band Reflectance: R_{NIR} [%]	Total Solar Reflectance: R_{tot} [%]
d = 25 nm	5.9	45.1	16.6	28.9
d = 50 nm	10.2	74.3	41.5	55.4
d = 100 nm	**13.3**	85.6	73.4	78.0
d = 200 nm	5.4	**85.7**	91.3	87.7
d = 400 nm	5.1	81.3	**95.1**	**87.9**
d = 800 nm	4.7	77.4	94.1	85.6

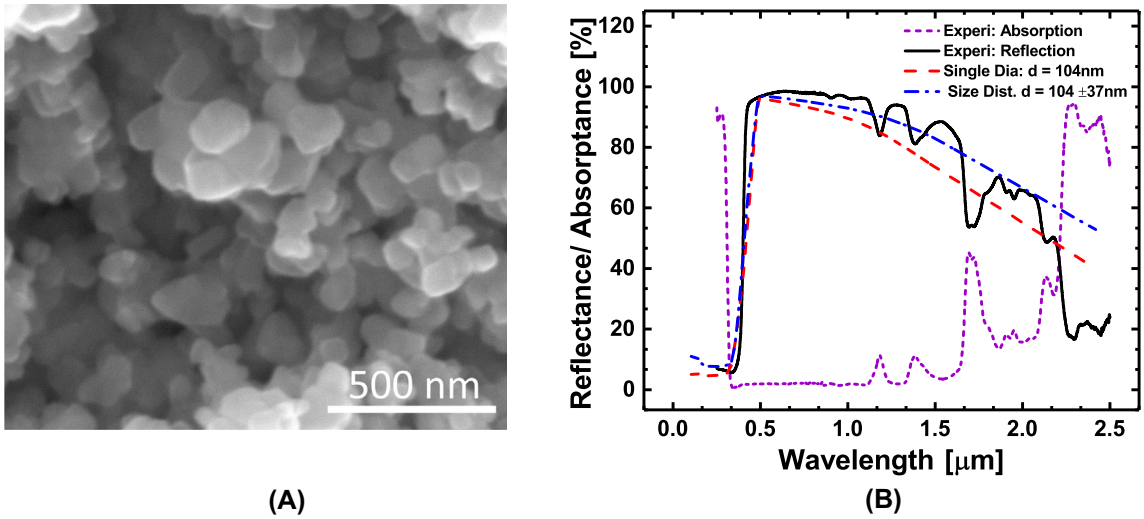

Fig. 5. (A) SEM of TiO_2 nanoparticles used in the experiment. (B) Single size, size distribution, and the experimental data on the spectral reflectivity of TiO_2 at a fixed volume fraction, $f = 8\%$, and 2 mm thickness embedded in an acrylic matrix, as well as the absorptance of pure acrylic to illustrate where the oscillations originate.

concentration to be 8%. Our results show that $\sigma = \pm$ 37 nm can increase the reflectance and greatly decreased the deviation of the experimental and modeling results, as seen in Fig. 5B. The size distribution model led to a total solar reflectance of 89.0%, which is ~1% deviation from the experimental results. The purple dotted line in Fig. 5B is the absorptance of the pure acrylic matrix sample to prove that the valleys in the experimental data are due to the absorption of the acrylic matrix of the sample rather than the TiO_2, thus the modeling will not capture these results due to our Mie Theory calculations not accounting for the matrix absorption.

3.3. Nanocomposites with multiple particle sizes

Recognizing that the solar spectrum is broad and motivated by the above results that a size dispersion increases reflectance, we explore intentionally using multiple sizes to maximizing solar reflectance. When considering what sizes to use, and their respective concentrations there are three main parameters to focus on: scattering coefficient, absorption coefficient, and phase function. The complex interplay of the three parameters yields the optimization of particle size distribution at a given total particle volume

Table 2
Particle size and respective volume fraction used for each model. The total volume fraction is conserved at 5% and the thickness of each model is 1 mm.

	Diameters [nm]	Volume Fractions [%]
A	25, 50, 100, 200, 400	0.25, 0.75, 3, 0.75, 0.25
B	25, 50, 100, 200, 400	0.75, 0.5, 1.75, 1.5, 0.5
C	50, 100, 200, 400, 800	0.2, 0.3, 1, 3, 0.5
D	100, 200, 300, 400, 600	0.2, 2.25, 0.5, 1.75, 0.3

concentration to be a nontrivial task. Here we will just demonstrate the concept using a manual trial-and-error based optimization, and further heuristic optimization could be done to find the actual optimal design. The first three models presented in this work were designed to optimize a certain reflectance value, i.e. the UV band, VIS band, or NIR band; and the fourth model was designed to optimize the total solar reflectance. The work is presented in such a way as to understand the contributions that the particle sizes and volume concentrations on the overall combination.

As mentioned in the previous section the smaller diameters are needed to reflect the shorter wavelengths, but in moderation due to their absorption, and larger diameters are needed to reflect the peak solar irradiation, $\lambda \approx 500$ nm. Considering the results in the earlier sections, we theoretically test four combinations of particles sizes, each combination is shown in Table 2. In Fig. 6 the scattering and absorption coefficients are plotted. Though the peaks of scattering coefficients of the combination of particles are lowered compared to the case with the single-size particles, a wider spectral range of scattering is achieved. The absorption coefficient is somewhat larger in the UV band, but this is somewhat of a tradeoff and is expected.

Fig. 7A shows the spectral reflectance over the entire solar region, while Fig. 7B shows the UV region and Fig. 7C shows the visible region. In Table 3, the reflection values for each band as well as the overall total solar reflection are reported for each multiple-size model. The spectral reflectance of each model outperforms any single particle size in the UV and VIS bands, as seen in Fig. 7A and B. Model A has a large portion of the total volume concentration on the smaller diameter particles leading to the greatest UV reflectance, also resulting in a loss in performance in the VIS and NIR, therefore, it is not an ideal combination for our system. Hence, its total solar reflectance is smaller than some of the single sizes. Model B resembles the reflectance curve of the 100 nm size particle with the majority of the volume concentration as 100 nm particles. It outperforms the 100 nm single size and Model A in that it gains considerably in the NIR and VIS bands with little sacrifice in the UV band. Model C introduces heavier weights of the mid-large particles and shows the greatest NIR reflectance, and Model D shows the greatest overall reflectance. Model D uses the larger particles, based on the results from Model C, and the midsized particles based on the results from Model B to achieve more uniform broad reflectance peak which leads to the greatest total solar reflection. These results clearly show that using particles of multiple sizes, when done correctly, can yield a greater reflection than any individual particle size on its own. For our applications, achieving the greatest overall solar reflection is desired, therefore the NIR and VIS bands are of the most interest because they contain >96% of the total solar irradiance. As shown in Fig. 4A, every single size has a characteristic reflection resonance, however putting all particles into one combination will eventually yield a diminishing marginal return at the resonance wavelength. By using multiple sizes, Model D enables multiple resonances and demonstrates greater reflectance in the NIR and VIS bands when compared to any single size. Furthermore, it is interesting to relate our findings to other relevant literature. For instance, an earlier study reported that using nanowire arrays of multiple diameters can enhance solar absorption as compared to a single diameter for photovoltaic applications [33]. Other works have reported using phonon scatters of multiple scales to reduce thermal conductivity for thermoelectric applications [34]. These findings, altogether, imply a general rule that when optimizing a transport property (be it reflectance, absorptance, or thermal conductivity) governed by a broad band of energy carriers (be it photons or phonons), hierarchical scatters or absorbers should be considered.

When searching this design space with a trial-and-error method, as demonstrated in this work, one should first consider what their target region of interest (ROI) is for reflection; for example, due to the dominant solar irradiation in the NIR region, this should be the first major ROI to be optimized. When selecting particle sizes and volume concentrations, a low absorption coefficient is the most significant contributor for reflectance, followed by the scattering coefficient peak location and particle's ability to backscatter. Once the optimal size is found for the greatest ROI, then additional particle sizes and volume concentrations are optimized for the secondary ROIs (i.e. VIS and UV in this work). The combination of these particles could lead to some sacrifice in the major ROI but should contribute to a greater global performance of the multi-size combination. Further iterations of the design space may be required as additional combinations should

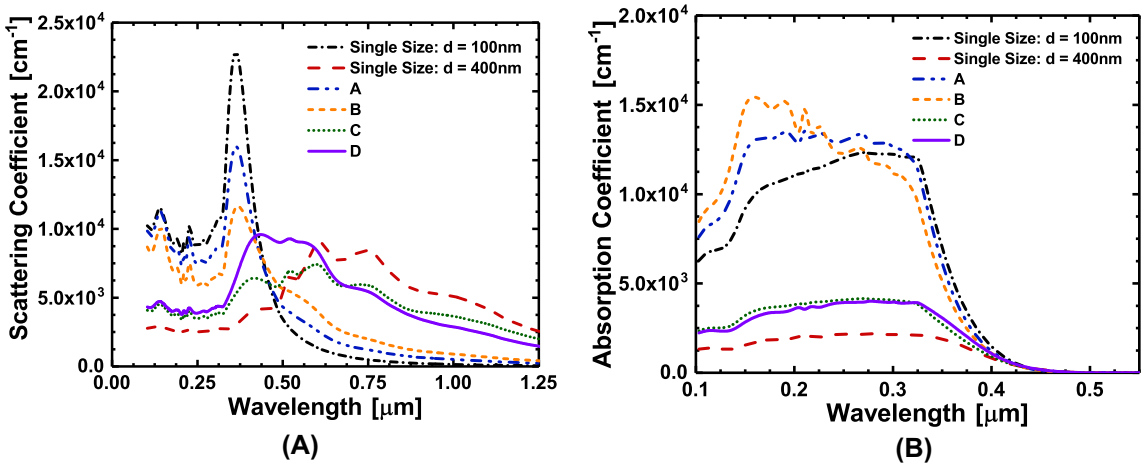

Fig. 6. (A) Scattering coefficient and (B) absorption coefficient for combinations of TiO_2 particles at a total volume fraction, $f = 5\%$ embedded in acrylic matrix.

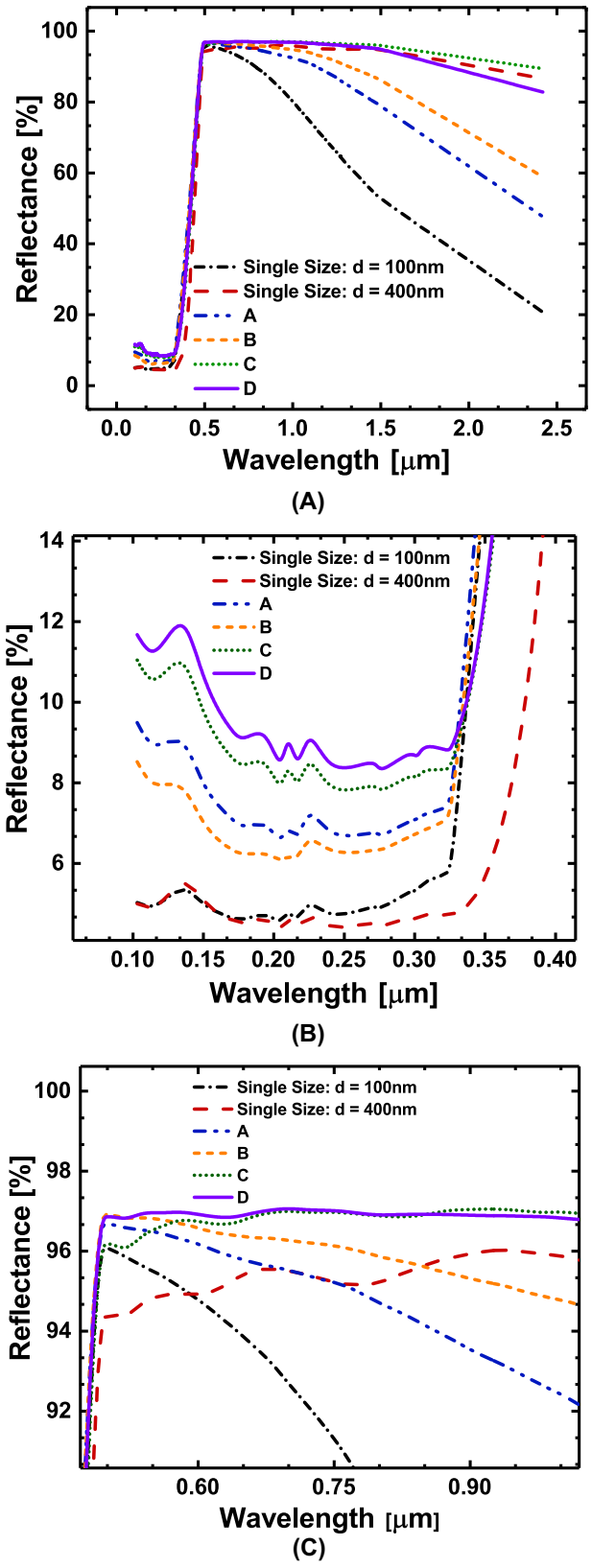

Fig. 7. (A) Spectral Reflectance of each model over the entire solar region, (B) Spectral Reflectance of each model over the UV region, (C) Spectral Reflectance of each model around the peak solar irradiation.

be introduced to find the maximum reflection. However, when considering these particle combinations, the impact of size and volume concentration leads to a diminishing return which is greatly dependent on the design space and constraints. We should note that our choices of multiple sizes and their volume fractions are still a proof-of-concept study, so it is not expected to yield the absolutely optimal design for maximum total solar reflection of TiO_2 nanocomposites. Various heuristic optimization techniques, including genetic algorithm or particle swarm optimization methods, may be used to further optimize our designs.

Table 3
Reflectance values for single size particles and multi-size combinations; the total volume fraction is conserved at 5% and the thickness of each model is 1 mm.

Model (Multi-Size)	UV Band Reflectance: R_{UV} [%]	VIS Band Reflectance: R_{VIS} [%]	NIR Band Reflectance: R_{NIR} [%]	Total Solar Reflectance: R_{tot} [%]
A	**14.7**	87.6	88.1	86.9
B	13.2	**87.7**	91.8	89.0
C	10.9	86.0	**96.5**	90.8
D	10.8	87.1	96.0	**91.0**

4. Conclusion

This work proposed the use of multiple-size particles in nanocomposites to enhance solar reflection to help aid the design for passive radiative cooling coatings. The results have shown that a combination of selected particle sizes and concentrations can expand the spectral scattering peaks while maintaining a relatively low absorption coefficient, leading to improvement in the spectral reflectivity across the entire solar spectrum and creating a greater total solar reflectance. In particular, introducing small particles with size 50–100 nm helps enhance the UV reflection, however, it negatively impacts the performance of the total solar reflection due to their strong absorption. Using moderate to large particle sizes, 150–600 nm, creates the broadest reflection peak over the portion of the solar spectrum with the largest intensities, making these sizes favorable for passive radiative cooling coatings. The simulation results show good agreement with the experimental data, validating the computational models. Though the motivation is passive radiative cooling technology, the findings may be used to a wide array of other applications. These findings will greatly enhance the cooling performance of dielectric nanocomposite coatings, potentially doubling their cooling power when compared to a single size particle. Moreover, our findings eliminate the need for precise control of particle size and may reduce the manufacturing cost of the coatings.

Conflicts of interest

The authors declare that there are no known conflicts of interest.

Acknowledgments

JP acknowledges the Laura Winkelman Davidson Endowment for partial support of this work; JP, XL, and XR acknowledge the Cooling Technologies Research Center (CTRC) for partial support of this work as well.

Appendix A. Supplementary material

Supplementary data associated with this article can be found, in the online version, at https://doi.org/10.1016/j.ijheatmasstransfer.2018.11.059.

References

[1] U.S.E.I. Administration, Annual Energy Outlook 2018 with projections to 2050, (2018) 1–64. http://doi.org/DOE/EIA-0383(2017).

[2] C.M. Lewandowski, N. Co-investigator, C.M. Lewandowski, Infrared Spectrosc. Conserv. Sci. (2015), https://doi.org/10.1017/CBO9781107415324.004.

[3] A.P. Raman, M.A. Anoma, L. Zhu, E. Rephaeli, S. Fan, Passive radiative cooling below ambient air temperature under direct sunlight, Nature 515 (2014) 540–544, https://doi.org/10.1038/nature13883.

[4] A.R. Gentle, G.B. Smith, A subambient open roof surface under the mid-summer sun, Adv. Sci. 2 (2015) 2–5, https://doi.org/10.1002/advs.201500119.

[5] Y. Zhai, Y. Ma, S.N. David, D. Zhao, R. Lou, G. Tan, R. Yang, X. Yin, Scalable-manufactured randomized glass-polymer hybrid metamaterial for daytime radiative cooling, Science (80-.) 7899 (2017) 1–9, https://doi.org/10.1126/science.aai7899.

[6] J. Kou, Z. Jurado, Z. Chen, S. Fan, A.J. Minnich, Daytime radiative cooling using near-black infrared emitters, ACS Photonics. acsphotonics.6b00991 (2017), https://doi.org/10.1021/acsphotonics.6b00991.

[7] H. Bao, C. Yan, B. Wang, X. Fang, C.Y. Zhao, X. Ruan, Double-layer nanoparticle-based coatings for efficient terrestrial radiative cooling, Sol. Energy Mater. Sol. Cells. 168 (2017) 78–84, https://doi.org/10.1016/j.solmat.2017.04.020.

[8] A.W. Harrison, Radiative cooling of TiO2 white paint, 20 (1978) 185–188.

[9] A. Andretta, B. Bartoli, B. Coluzzi, V. Cuomo, A. Andretta, B. Bartoli, B. Coluzzi, V. C. Selective, S. For, Selective surfaces for natural cooling devices, J. Phys. Colloq. 42 (1981), C1–423-C1-430.

[10] T.M.J. Nilsson, G.A. Niklasson, Radiative cooling during the day: simulations and experiments on pigmented polyethylene cover foils, Sol. Energy Mater. Sol. Cells. 37 (1995) 93–118, https://doi.org/10.1016/0927-0248(94)00200-2.

[11] Z. Huang, X. Ruan, Nanoparticle embedded double-layer coating for daytime radiative cooling, Int. J. Heat Mass Transf. 104 (2017) 890–896, https://doi.org/10.1016/j.ijheatmasstransfer.2016.08.009.

[12] S. Atiganyanun, J.B. Plumley, S.J. Han, K. Hsu, J. Cytrynbaum, T.L. Peng, S.M. Han, S.E. Han, Effective radiative cooling by paint-format microsphere-based photonic random media, ACS Photonics 5 (2018) 1181–1187, https://doi.org/10.1021/acsphotonics.7b01492.

[13] P. Yang, C. Chen, Z.M. Zhang, A dual-layer structure with record-high solar reflectance for daytime radiative cooling, Sol. Energy. 169 (2018) 316–324, https://doi.org/10.1016/j.solener.2018.04.031.

[14] J.C. Maxwell, B.A. Garnett, Colours in Metal Classes and in Metallic Films, 203 (1904) 385–420.

[15] C.F. Bohren, D.R. Huffman, Absorption and scattering of light by small particles, Wiley, 2004.

[16] M.F. (Michael F. Modest, Radiative heat transfer, Elsevier Science, 2013.

[17] J.R. Frisvad, N.J. Christensen, H. Wann Jensen, Computing the scattering properties of participating media using Lorenz-Mie theory, ACM Trans. Graph. Artic. 26 (2007), https://doi.org/10.1145/1239451.1239511.

[18] Y. Lin Xu, B.Å.S. Gustafson, A generalized multiparticle Mie-solution: Further experimental verification, J. Quant. Spectrosc. Radiat. Transf. 70 (2001) 395–419, https://doi.org/10.1016/S0022-4073(01)00019-X.

[19] J.R. Howell, R. Siegel, M.P. Mengüç, Thermal radiation heat transfer, n.d.

[20] T. Wriedt, The Mie Theory 169 (2012), https://doi.org/10.1007/978-3-642-28738-1.

[21] H.C. van de Hulst, Light scattering by small particles, Courier Corporation (1957).

[22] M. Kerker, The Scattering of Light and Other Electromagnetic Radiation, Academic Press, 1969.

[23] W. Sun, N.G. Loeb, Q. Fu, Light scattering by coated sphere immersed in absorbing medium: a comparison between the FDTD and analytic solutions, J. Quant. Spectrosc. Radiat. Transf. 83 (2004) 483–492, https://doi.org/10.1016/S0022-4073(03)00101-8.

[24] M. Baneshi, S. Maruyama, A. Komiya, Infrared radiative properties of thin polyethylene coating pigmented with titanium dioxide particles, J. Heat Transf. 132 (2010), https://doi.org/10.1115/1.4000235, 023306-023306.

[25] W.C. Mundy, J.A. Roux, A.M. Smith, Mie scattering by spheres in an absorbing medium, J. Opt. Soc. Am. 64 (1974) 1593, https://doi.org/10.1364/JOSA.64.001593.

[26] W.B. Gordon, Far-field approximations to the Kirchhoff-Helmholtz representations of scattered fields, IEEE Trans. Anten. Propag. 55 (2014) 2844–2851, https://doi.org/10.1109/TAP.1975.1141105.

[27] P. Chylekt, Light scattering by small particles in an absorbing medium, J. Opt. Soc. Am. 67 (1977) 561–563.

[28] M.A. Gali, A.R. Gentle, M.D. Arnold, G.B. Smith, Extending the applicability of the four-flux radiative transfer method, Appl. Opt. 56 (2017) 8699, https://doi.org/10.1364/AO.56.008699.

[29] C. Mätzler, MATLAB functions for Mie scattering and absorption, Inst. Für Angew. Phys. (2002) 1–19.

[30] R. Vaillon, B.T. Wong, P. Mengüç, Polarized radiative transfer in a particle-laden semi-transparent medium via a vector Monte Carlo method, J. Quant. Spectrosc. Radiat. Transf. 84 (2004) 383–394, https://doi.org/10.1016/S0022-4073(03)00257-7.

[31] L. Wang, S. Jacques, Monte Carlo modeling of light transport in multi-layered tissues in standard C, Univ. Texas. (1992) 1–167.

[32] ASTM, Standard tables for reference solar spectral irradiances: Direct normal and, ASTM Int. 03 (2012) 1–21, https://doi.org/10.1520/G0173-03R12.2.

[33] H. Bao, X. Ruan, Optical absorption enhancement in disordered vertical silicon nanowire arrays for photovoltaic applications, Opt. Lett. 35 (2010) 3378–3380, https://doi.org/10.1364/OL.35.003378.

[34] K. Biswas, J. He, I.D. Blum, C.I. Wu, T.P. Hogan, D.N. Seidman, V.P. Dravid, M.G. Kanatzidis, High-performance bulk thermoelectrics with all-scale hierarchical architectures, Nature 489 (2012) 414–418, https://doi.org/10.1038/nature11439.